Check for updates

Synthesis and photophysical properties of BODIPY-decorated graphene quantum dot–phthalocyanine conjugates†

Nnamdi Nwahara, Reitumetse Nkhahle, Bokolombe P. Ngoy, John Mack [iD] and Tebello Nyokong [iD] *

This work reports on the synthesis and characterisation of novel supramolecular hybrids containing BODIPY-decorated graphene quantum dots (BODIPY@GQDs) and zinc phthalocyanine. Graphene quantum dots (GQDs) were functionalized with L-glutathione (GSH) in order to assist coupling to the BODIPY dye. {2,9(10)16(17)23(24)-Tetrakis-[3-(diethylamino)phenoxy]phthalocyaninato}zinc(II) (**1**) was immobilized *via* π−π stacking interaction on the BODIPY-decorated GQDs and pristine GQDs to form the supramolecular hybrids **1**-BODIPY@GQDs and **1**-GQDs, respectively. The photophysical and photochemical properties of these conjugates were investigated. Energy transfer occurred from the (i) GQDs to BODIPY, (ii) GQDs to **1**, and (iii) BODIPY@GQDs to **1** *via* fluorescence resonance energy transfer (FRET). The highest FRET efficiency was observed for the BODIPY@GQDs (0.93). The introduction of the BODIPY core to the GQD structure resulted in higher triplet, and singlet oxygen quantum yields for the resultant Pc/GQD hybrid (**1**-BODIPY@GQDs). The zeta potential values obtained imply a high colloidal stability for the supramolecular hybrids. The results suggest that such hybrids may be applied in fields such as photodynamic therapy (PDT), where a high singlet oxygen quantum yield is desired.

Introduction

Phthalocyanines (Pcs) are a class of highly conjugated π-electron systems with excellent physical and chemical properties.[1] These unique properties have led to their wide range of applications in fields such as catalysis and sensing.[2–5] Recently, interest has grown in the application of metallophthalocyanines (MPcs) as photosensitizers for photodynamic therapy (PDT) owing to their distinctive intense absorption in the red region of the visible spectrum.[6,7] This is because body tissue is passably transparent in this spectral region and hence photosensitizers absorbing in this region are more effective for PDT.[6–8]

Photodynamic therapy is a non-invasive therapeutic modality, which employs the combined action of a photosensitizer and specific light sources for the treatment of various cancers.[9,10] Upon activation by light, the electronically excited photosensitizer transfers its energy to ground state molecular oxygen to produce excited singlet oxygen, the chief cytotoxic species which initiates an irreversible photo-damage of tumour cells.[11,12]

Borondipyrromethenes (BODIPYs), like Pcs, are photosensitizers for PDT,[13,14] with a number of desirable properties, including low dark toxicity ratios, resistance to harsh environments and high extinction coefficients.[15–17] There are many individual examples of BODIPYs and phthalocyanines, but only a few hybrid structures have been reported.[18–20] These hybrids have been shown to have superior properties compared to their constituent structures with high singlet oxygen quantum yields.[18–20] The current work reports on a composite containing BODIPY, MPc and graphene quantum dots (GQDs) as a platform for potential use in PDT.

Nanoparticle (NP)-based drug delivery systems have provided an unprecedented opportunity in cancer treatment for improved drug loading, targeting and efficacy.[21,22] Among these nanoparticles, graphene quantum dots have gained considerable interest as carbon-based nanomaterials characterized by robust chemical inertness, low toxicity, and high solubility in both aqueous and non-aqueous solvents.[23,24] These properties have made the GQDs attractive alternatives to semiconductor QDs for use in a number of applications, including bio imaging, sensing, photocatalysis, as well as drug delivery.[25–28] Their large surface area affords them impressive drug loading potential, with up to 200% loading capacity reported.[29] Moreover, GQDs are known PDT agents with high singlet oxygen quantum yields.[30]

Department of Chemistry, Rhodes University, Grahamstown 6140, South Africa.
E-mail: t.nyokong@ru.ac.za; Tel: +27 46 6038260

† Electronic supplementary information (ESI) available: NMR spectra, absorption spectra, emission spectra, EDX spectra, input *vs.* output plot and singlet oxygen plot. See DOI: 10.1039/c8nj00758f

In this work, we combine the three PDT agents with the aim of improving PDT activity by the synergistic effect. Conjugates of MPc with GQDs have previously been reported.[31,32] To the best of our knowledge, BODIPY decorated GQDs are not known and are thus reported for the first time in this work. By conjugating the BODIPY to the GQDs and then linking the resulting conjugate to a Pc, this work seeks to fabricate Pc/GQD/BODIPY hybrids with improved energy transfer properties, and hence PDT potential. Following the linking of BODIPY to GQDs (to form BODIPY@GQDs), the Pc will be assembled on the BODIPY@GQDs through π–π stacking between the GQDs and the Pc, since both have extensive π bonds. This work envisaged that the anchoring of dyes such as BODIPYs and phthalocyanines to GQDs could result in composites which exhibit properties superior to the individual molecules.

This work therefore, reports on the synthesis and photophysical properties of novel BODIPY-decorated GQDs, and their supramolecular hybrids with phthalocyanines. The Pc employed in this work is the {2,9(10)16(17)23(24)-tetrakis-[3-(diethylamino)-phenoxy]phthalocyaninato}zinc(II) (1), which has been previously reported.[33] Zn is employed as a central metal since ZnPc has good singlet oxygen generating abilities.

Experimental

Materials

1,3-Diphenylisobenzofuran (DPBF), quinine sulfate, 2,4-dimethyl-3-ethylpyrrole, 4-formylbenzoic acid, rhodamine 6G, trifluoro acetic acid (TFA), tetrachloro-1,4-benzoquinone(p-chloranil), boron trifluoride diethyl etherate (BF$_3$·OEt$_2$), magnesium sulphate, triethylamine, and N-hydroxysuccinimide (NHS) were obtained from Sigma-Aldrich. N,N′-Dicyclohexylcarbodiimide (DCC) was purchased from Merck. Dimethyl sulfoxide (DMSO) N,N-dimethylformamide (DMF), and dichloromethane (DCM) were obtained from SAARCHEM. All aqueous solutions were prepared using ultra-pure water obtained from a Milli-Q Water system (Millipore Corp., Bedford, MA, USA). All other reagents and solvents were obtained from commercial suppliers and were of analytical grade and used as received. Complex 1 was synthesized and purified as reported in the literature.[33] Glutathione (GSH) capped GQDs (GQDs@GSH) were synthesized as reported in the literature.[32]

Equipment

Excitation and emission spectra were recorded on a Varian Eclipse spectrofluorimeter. Ground state electronic absorption spectra were recorded on a Shimadzu UV-2550 spectrophotometer. Infrared (FTIR) spectra were recorded on a Bruker Alpha IR (100 FT-IR) spectrophotometer. ^{1}H and ^{13}C NMR spectra were recorded on Bruker® AVANCE II 400 MHz NMR spectrometer using tetramethylsilane (TMS) as an internal reference. X-ray powder diffraction (XRD) patterns were recorded on a Bruker D8 Discover equipped with a Lynx-Eye Detector, using Cu Kα radiation (= 1.5405 Å, nickel filter) as previously described.[34] Transmission electron microscopy (TEM) micrographs were

obtained using a Zeiss Libra 120 TEM operating at 80 kV. Energy dispersive X-ray spectroscopy (EDS) was done on an INCA PENTA FET coupled to the VAGA TESCAM using 20 kV accelerating voltage. Dynamic light scattering (DLS) experiments were done on a Malvern Zetasizer nanoseries, Nano-ZS90. A Bruker Vertex 70-Ram II Raman spectrometer (equipped with a 1064 nm Nd:YAG laser and liquid nitrogen cooled germanium detector) was used to collect Raman spectral data. A laser flash photolysis system was used for the determination of the decay kinetics. Samples were prepared in deoxygenated DMSO by bubbling with argon for 15 min. The excitation pulses (3–5 ns) were produced by an EKSPLA NT342N-20-AW tunable wavelength laser. Fluorescence lifetimes were measured using a time-correlated single photon counting (TCSPC) setup (Fluo Time 300, Picoquant GmbH), details have been provided before.[32] Photo irradiation for singlet oxygen determinations was done using a General Electric Quartz line projector lamp (300 W). A 600 nm glass cut off filter (Schott) and a water filter were used to filter off ultraviolet and infrared radiations, respectively. An interference filter (Intor, 670 nm with a bandwidth of 40 nm) was additionally placed in the light path before the sample. Light intensities were measured with a POWER MAX5100 (Molelectron detector incorporated) power meter and were found to be 2.97×10^{16} photons^{-1} cm^{-2}.

Synthesis

Synthesis of carboxylic acid BODIPY (Scheme 1)

The synthesis of the BODIPY dye was carried out according to reported methods[35] with slight modifications (Scheme 1). Firstly, to a solution of 2,4-dimethyl-3-ethylpyrrole (2 g, 16.2 mmol) in dry dichloromethane (100 mL), 4-formylbenzoic acid (1.2 g, 8.1 mmol) was added followed by 3 drops of trifluoro acetic acid under N$_2$. The mixture was stirred for 3 h. The reaction mixture was cooled at 0 °C while p-chloranil (2.34 g, 9.52 mmol) was added and the stirring continued for 1 h. Triethylamine (TEA, 10 mL) and boron trifluoride diethyl etherate (10 mL) were added at 0 °C and the reaction mixture was stirred overnight at room temperature. The crude product was filtered, washed with water (30 × 50 mL) and the organic layer was dried over MgSO$_4$, and then the solvent evaporated.
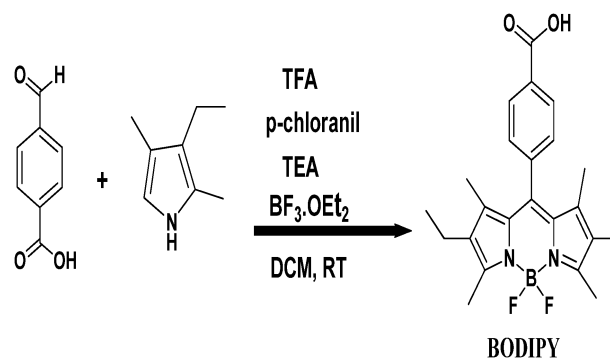
Scheme 1 The synthetic procedure for the BODIPY dye.

The desired compound was obtained after purification *via* column chromatography using dichloromethane and ethyl acetate (2:1) with 40% yield (w/w); UV-vis (DMSO) λ_{max}/nm (log$_\epsilon$): 523 (5.11). ^{1}H NMR (600 MHz, acetone) 8.27 (d, 2H, Ar-H), 7.59 (d, 2H, Ar-H), 2.52 (s, 6H, –CH$_3$), 2.43–2.29 (m, 4H, –CH$_2$), 1.35 (s, 6H, –CH$_3$), 1.01 (s, 6H, –CH$_3$) ppm. ^{13}C NMR (151 MHz, acetone) 166.18, 153.92, 140.32, 139.56, 138.09, 132.96, 131.17, 130.45, 128.83, 16.56, 13.9, 11.71, 11.13 ppm.

Conjugation of BODIPY to GQDs (Scheme 2)

BODIPY decorated GQDs (BODIPY@GQDs) were prepared as follows: a mixture of the as-synthesized BODIPY (20 mg, 0.047 mmol) was dissolved in DMSO (3 mL). Then DCC (0.02 g, 0.098 mmol) and NHS (0.015 g, 0.13 mmol) were added and the resultant solution was stirred for 48 h under gentle stirring in order to activate the carboxylic groups of the BODIPY, following which GQDs@GSH (10 mg) was added and the mixture further stirred for 48 h. The resulting conjugate (BODIPY@GQDs) was precipitated out from solution with trifluoroacetic acid (TFA) and ice. The precipitate was washed several times with water,

centrifuged, and then dried in a fume hood to obtain the BODIPY@GQDs (Scheme 2).

Attachment of complex 1 to GQDs to form 1-GQDs

Adsorption of complex **1** to the GQD surface is through the π–π stacking interaction. This conjugate was prepared following methods previously described for the noncovalent (adsorption) of other Pcs to GQDs with some modification.[32] Firstly, GQDs (10 mg mL^{-1}) in 2 mL DMF were added to **1** (30 mg, 0.024 mmol) in 2 mL DMF. The GQDs and complex **1** mixture was ultrasonicated for 4 h, followed by stirring for 4 days. The green colour of the Pc turned light green due to adsorption to GQDs. It is expected that not all of GQDs and complex **1** will form conjugates, and the unreacted starting materials were removed by washing repeatedly with ethanol. The solid product was dried in a fume hood to obtain **1**-GQDs conjugates.

Attachment of complex 1 to BODIPY@GQDs to form 1-BODIPY@GQDs

Non-covalent coordination (π–π stacking) of BODIPY@GQDs to complex **1** was according to methods reported above with a
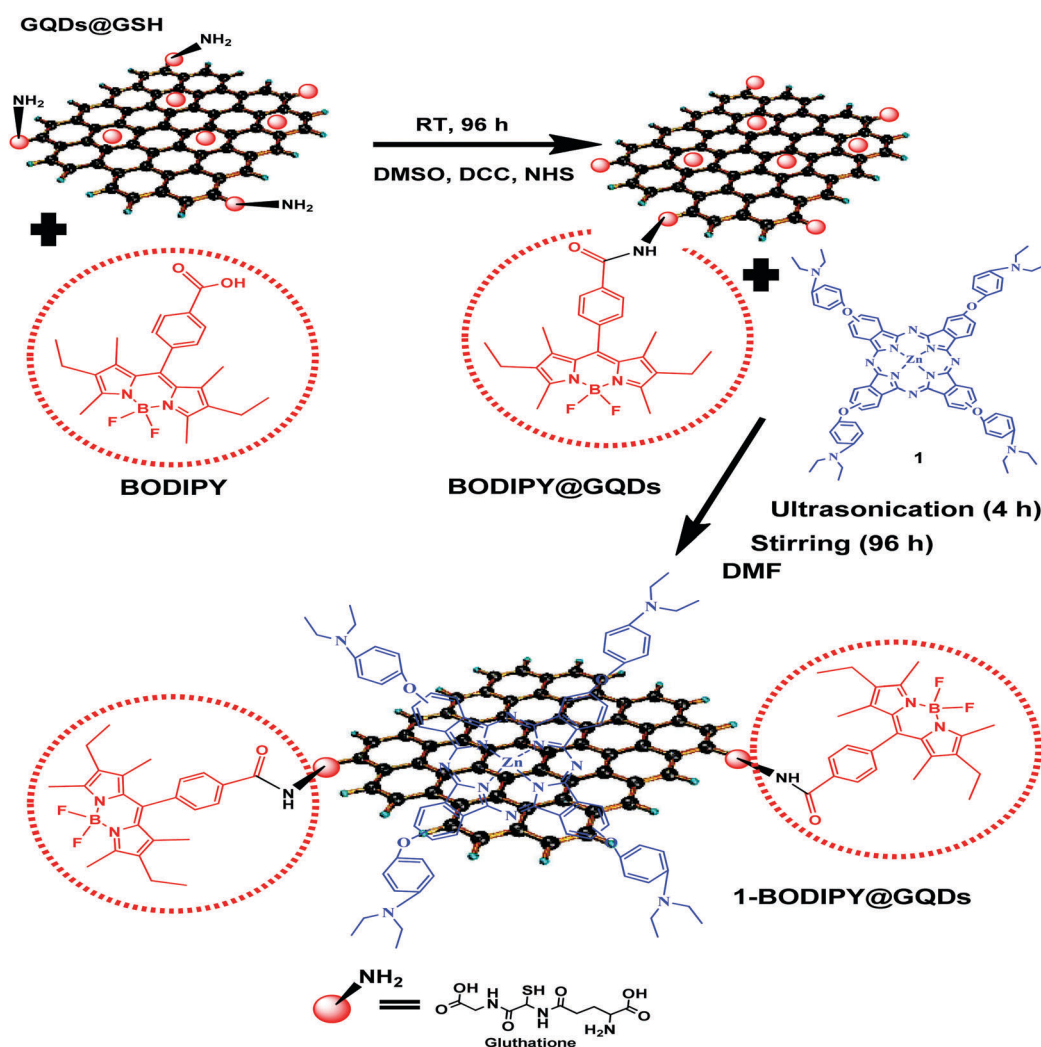
Scheme 2 Schematic for the preparation of BODIPY-functionalized graphene quantum dots with illustration of the π–π stacking of GQDs and complex **1**.

slight modification.[32] Briefly: 10 mg mL^{-1} of BODIPY@GQDs was added to **1** (30 mg, 0.024 mmol), in 5 mL of dry DMF. The resultant mixture was ultrasonicated for 4 h; followed by stirring in the dark for 96 h. The resultant conjugate was precipitated out of solution with ethanol, and repeatedly washed with water to ensure that uncomplexed BODIPY@GQDs and Pcs were eliminated. Again, not all of the BODIPY@GQDs will form conjugates with complex **1**, hence the need for purification. The solid products were then dried under vacuum and are represented as **1**-BODIPY@GQDs.

Photophysical and photochemical parameters

The fluorescence (Φ_F), singlet oxygen (Φ_Δ) and triplet (Φ_T) quantum yields were assessed using the comparative methods reported in the literature,[1,36,37] using the following standards: rhodamine 6G ($\Phi_F = 0.92$ in ethanol)[38] and Rose Bengal ($\Phi_\Delta^{std} = 0.76$ in DMSO)[39] when exciting where BODIPY absorbs and quinine sulfate in H$_2$SO$_4$ (0.05 M) ($\Phi_F = 0.52$)[38] when exciting where the GQDs absorb. Unsubstituted ZnPc in DMSO was employed when exciting where MPc absorbs with the following reference values: ($\Phi_F = 0.20$),[37] ($\Phi_\Delta^{std} = 0.67$),[1] and ($\Phi_T^{std} = 0.65$).[40] DPBF was used as a singlet oxygen quencher for BODIPY and complex **1**. The singlet oxygen quantum yield (Φ_Δ) determination of the MPc and BODIPY complexes was determined using the photochemical methods reported before.[1] The concentration of DPBF was lowered to 3×10^{-5} mol dm^{-3} for all solutions, to avoid chain reactions. DPBF degradation was spectroscopically monitored at 417 nm at predetermined time intervals. The fluorescence quantum yields of the GQDs in the conjugates (BODIPY@GQDs, **1**-GQDS, and **1**-BODIPY@GQDs) and BODIPY in the conjugates (BODIPY@GQDs and **1**-BODIPY@GQDs), ($\Phi_{F(GQDs/BODIPY)}^{Conjugate}$) were calculated using eqn (1).

$$\Phi_{F(GQDs/BODIPY)}^{Conjugate} = \Phi_{F(GQDs/BODIPY)} \frac{F_{GQDs/BODIPY}^{Conjugate}}{F_{GQDs/BODIPY}} \quad (1)$$

where $\Phi_{F(GQDs/BODIPY)}$ is the fluorescence quantum yield of the pristine GQD or BODIPY alone and was used as a standard. $F_{GQDs/BODIPY}$ is the fluorescence intensity of the GQDs or BODIPY alone and $F_{GQDs/BODIPY}^{Conjugate}$ and when conjugated to complex **1**.

Results and discussion

Synthesis and characterization

The synthetic route for the carboxylic acid BODIPY is illustrated in Scheme 1. The synthesis of the BODIPY generally involves the condensation of 2,4-dimethyl-3-ethylpyrrole and 4-formylbenzoic acid under reflux in dichloromethane, followed by treatment of the reaction mixture with triethylamine and boron trifluoride diethyl etherate. The structure and purity of the synthesized BODIPY was confirmed by UV-vis, ^{1}H NMR, ^{13}C NMR, and FTIR data which were in agreement with the proposed structure. The ^{1}H NMR spectrum for the carboxylic BODIPY is shown in Fig. S1A (ESI†). The aromatic and aliphatic protons were observed between 8.27–7.59 ppm and 2.43.0–1.01 ppm, respectively.

The carbonyl and aromatic carbons were observed between 166 and 128 ppm and, aliphatic carbons between 16–11 ppm in the ^{13}C NMR spectra as illustrated in Fig. S1B (ESI†). The as-synthesized BODIPY dye exhibits high molar absorption coefficients ($\sim$129 532 M^{-1} cm^{-1}) and hence is a suitable donor molecule due to its high light harvesting properties (Fig. S2, ESI†).

The successful conjugation of BODIPY to GQDs to give BODIPY@GQDs was confirmed using FTIR. The FTIR spectrum of the BODIPY@GQDs (Fig. 1(c)) shows the presence of an amide peak between 3600 and 3000 cm^{-1}. The primary amine and primary amides are known to have two "fangs", while the secondary amines and amides have a single peak. The FTIR spectrum of the GQDs@GSH (Fig. 1(a)) shows the presence of two peaks at 3360 and 3217 cm^{-1}. It can be observed that upon linkage of the GQDs to the BODIPY, the two peaks disappear, with the appearance of a new single peak at 3321 cm^{-1}. The disappearance of the two peaks (N–H) is a result of the chemical bonding of the carboxyl group of the BODIPY to the amino group of the GQDs. The emergence of a new single peak at 3321 cm^{-1} confirms the successful conjugation and hence formation of the resultant BODIPY@GQDs. Moreover, shifts in the C=O peak positions from 1683 cm^{-1} in the BODIPY dye (Fig. 1(b)) to 1616 cm^{-1} in the conjugate (BODIPY@GQDs) (Fig. 1(c)) also confirms the formation of an amide bond between the GQDs and the BODIPY dye, and hence formation of the BODIPY@GQDs.
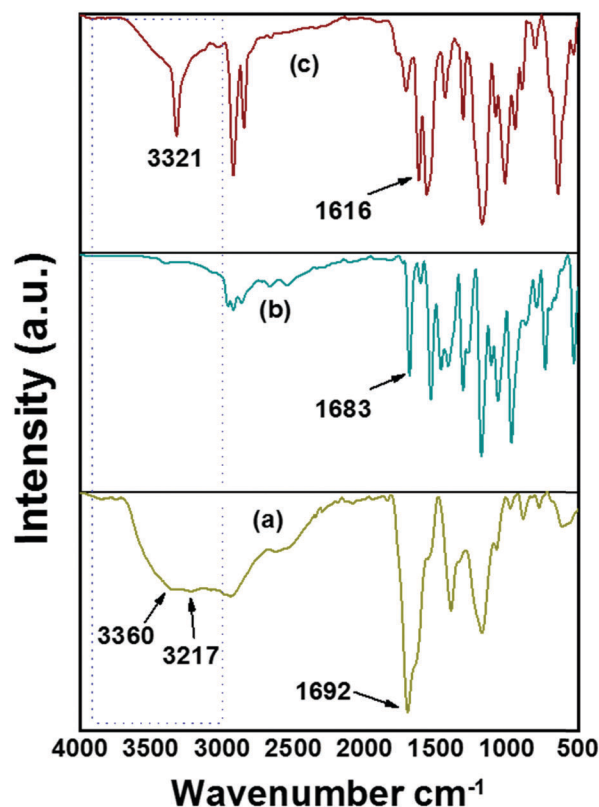

Fig. 1 FTIR spectra of (a) GQDs@GSH, (b) BODIPY, and (c) BODIPY@GQDs showing amide bond formation.
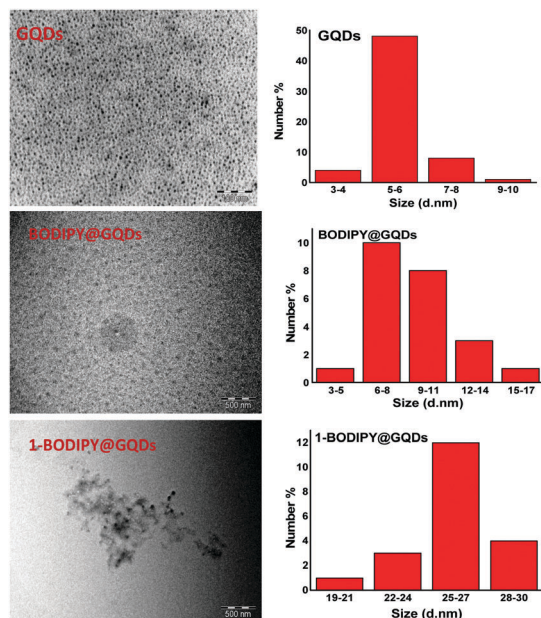
Fig. 2 TEM images of GQDs, BODIPY@GQDs, and **1**-BODIPY@GQDs showing changes in size upon modifications with the corresponding size distributions (histograms) under the TEM images.

Transmission electron microscopy (TEM) was used to assess the morphologies of the GQDs, BODIPY@GQDs and **1**-BODIPY@GQDs. Fig. 2 shows the representative TEM image of GQDs, showing their monodispersed nature with an overall quasi-spherical morphology and a particle size average of about 5 nm. There were slight changes in particle sizes observed on going from GQDs at 5 nm to BODIPY@GQDs and **1**-BODIPY@GQDs at 8 nm and 25 nm, respectively (Fig. 2).

The increase in size following conjugation confirms the successful modification at each stage attributable to aggregation,[41–43] which is possible in both phthalocyanines and BODIPYs through π–π interaction of these respective dyes on adjacent NPs.

The qualitative determination of the elemental composition of the complex **1** and the BODIPY with or without GQDs were evaluated using an energy dispersive X-ray spectrometer (EDX) (Fig. S3, ESI†). The results obtained were consistent with the expected elemental composition for complex **1** and the BODIPY. On conjugation additional peaks (S and N) from the GQDs were observed. The presence of C, N, O, S, B and F, and C, N, O, S, B, F, and Zn for BODIPY@GQDs and **1**-BODIPY@GQDs, respectively, signified the successful formation of these composites.

Dynamic light scattering (DLS) analysis revealed average hydrodynamic sizes of 5.5 nm, 11.0 nm, 21.0 nm and 28.2 nm for the GQDs, BODIPY@GQDs, **1**-GQDs and **1**-BODIPY@GQDs (Fig. 3), Table 1. These results show that following conjugation, the hydrodynamic diameters of the GQDs increased, which further suggests successful formation of desired complexes. The observed changes in size of the GQDs alone following modification seen in DLS plots were also observed above using TEM.

Zeta potential is a measure of the charges carried by particles suspended in a liquid (mostly water). It is an important parameter in the fabrication of supramolecular structures as a high zeta potential confers colloidal stability. Zeta-potential measurements for the GQDs alone gave a value of −18.1 mV indicative of highly negative surface charges. This is due to the presence of carboxyl and hydroxyl groups in the GQDs.[44] The Pc alone had a low positive zeta potential of 6.7 mV. However, hybridization with GQDs and BODIPY@GQDs, resulted in an increase (compared to complex **1**) in the electrostatic repulsions and therefore stability (for **1**-GQDs and **1**-BODIPY@GQDs, with zeta potential values of −18.7 mV and −16.5 mV, respectively), Table 1. Moreover, the high zeta potential values following hybrid formation points to improvements in the dispersibility of the resulting supramolecular structures, signifying high
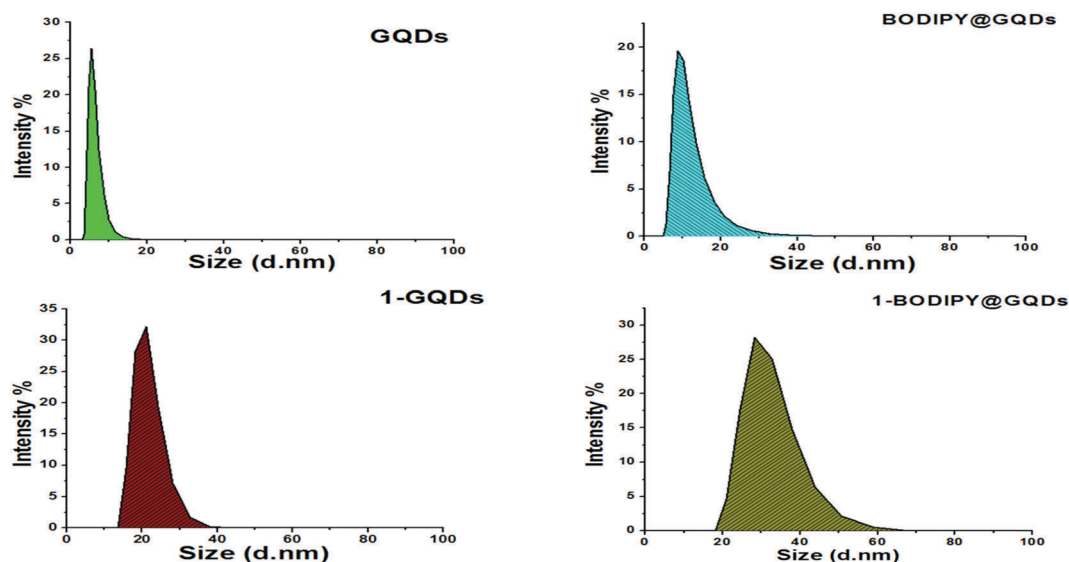

Fig. 3 Representative DLS graphs showing average particle sizes for GQDs alone, BODIPY@GQDs, **1**-GQDs, and **1**-BODIPY@GQDs.

Table 1 Photophysicochemical data of complex **1** and conjugates in DMSO

Compound	Size (nm) from DLS[a]	Zeta potential[a] (mV)	λ_{abs}[b] (nm)	Dye-loading (µg Pc mg^{-1} NPs)	Φ_F[b]	τ_f[b] (ns)	τ_{isc} (ns)	FRET Eff	Φ_T	T_T (µs)	Φ_Δ
1	—	6.7	683	—	0.03	1.02	1.59	—	0.63	322	0.50
1-GQDs	21.0 (5.5)	−18.7 (−18.1)	682 (332)	20	0.01 (0.23)	0.89 (2.84)	1.33	0.76	0.67	221	0.58
BODIPY	—	−6.4	[525]	—	[0.85]	[5.05]	—	—	—	—	0.10
BODIPY@GQDs	11.0 (5.5)	−11.6	[526] (335)	13	[0.60] (0.02)	[4.85]*	—	0.93	—	—	0.28
1-BODIPY@GQDs	28.2	−16.5	681 [527] (340)	26	<0.01 [0.55] (0.10)	0.78 [4.76]*	1.00	0.84	0.78	177	0.70

[a] Values in brackets are for GQDs alone. [b] Values in round brackets are for the GQD component, and values in square brackets are for the BODIPY component. Otherwise, values are for complex **1**. The fluorescence quantum yield and lifetime value for GQDs@GSH alone are 0.27 and at 3.41 ns, respectively. The fluorescence lifetime values marked with * represents both BODIPY and GQDs, since both were excited.
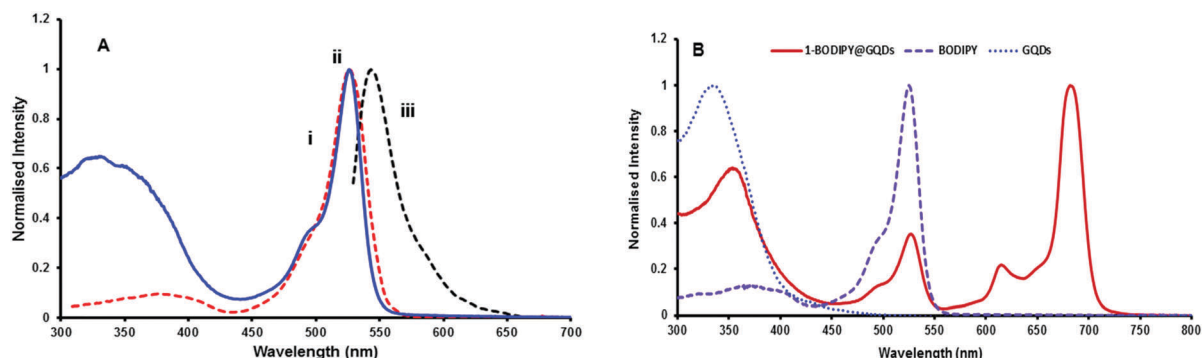

Fig. 4 (A) Absorption (i), excitation (ii), and emission (iii) spectra of BODIPY@GQDs, and (B) electronic absorption spectra for **1**-BODIPY@GQDs, BODIPY dye, and GQDs in DMSO.

colloidal stability. This property is very favourable for biological applications.[45]

Fig. S4 (ESI†) shows the normalized absorption, emission, and excitation spectra of the as-synthesized BODIPY and Fig. 4A for BODIPY@GQDs. As can be seen from the figures, the excitation spectra were found to be mirror images of the emission spectra, and the latter were the same as the absorption spectra. The closeness of the absorption and excitation spectral maxima, shows that the absorbing species is the same as the emitting one, and suggests that the BODIPY does not readily aggregate in solution.

The ground state absorption spectra of **1**-BODIPY@GQDs (Fig. 4B) showed characteristic absorptions for both complex **1**, BODIPY, as well as the GQD moieties. From the figure, the strong absorption below 400 nm is attributed to the presence of the GQDs and attributable to the n–π* electronic transitions caused by the oxygen containing groups on the surface of the GQDs.[46] For GQDs, the absorption band shifted from 332 nm for the GQDs alone to 335 nm for BODIPY@GQDs, and 340 nm for **1**-BODIPY@GQDs, Table 1. Shifts in peak positions for GQDs can be attributed to aggregation and hence increases in the size of the nanoparticles subsequent to conjugation with complex **1** (as illustrated by DLS sizes). There were no significant shifts in the absorption maximum of BODIPY in BODIPY@GQDs compared to the BODIPY alone (figure not shown). Insignificant shifts were observed for the Q band of complex **1** on coordination. The loading of complex **1** onto the nanoparticles was estimated following literature reports.[47] It involves comparing the absorbance intensities of either complex **1** or BODIPY before and after conjugation. This is then related to the respective molar absorptivity of complex **1** and BODIPY to determine loading. It must be noted that loading values in Table 1 are lower that the masses used in the Experimental section since as stated above not all the starting material formed the conjugates. A larger loading is observed for **1**-BODIPY@GQDs compared to **1**-GQDs. This may be due to the larger size of BODIPY@GQDs, allowing more Pcs to be loaded.

The crystalline structure GQDs alone and the nanocomposites were elucidated using X-ray diffraction (XRD) (Fig. 5). The GQDs exhibit a main (broad) diffraction peak at $2\theta = 25°$ (Fig. 5a) which is due to the (002) Bragg's reflection of the carbon in the graphene layers.[48] The broadness of the XRD peak for the GQDs reflects their small size and is consistent with previous structural analysis on GQDs.[48,49] The XRD pattern of the BODIPY (Fig. 5b) shows sharp peaks confirming the microcrystalline nature.[50] These peaks become pronounced post conjugation to GQDs (BODIPY@GQDs), Fig. 5c. The slight changes in crystal structure of the BODIPY upon conjugation to GQDs, suggests that modification of the GQDs with BODIPY affects the bulk composition.[51] It has been reported that changes in the degree of crystallization imply a new crystal form or a new compound in dye macrocycles.[52]

The broadness observed in the diffraction patterns of the complex **1** is indicative of an amorphous structure, which is typical of phthalocyanines, Fig. 5d.[53] Fig. 5e shows peaks due the phthalocyanine and additionally, microcrystalline peaks attributed to the presence of the BODIPY@GQDs in **1**-BODIPY@GQDs (Fig. 5e). For the **1**-GQDs (figure not shown) there were no
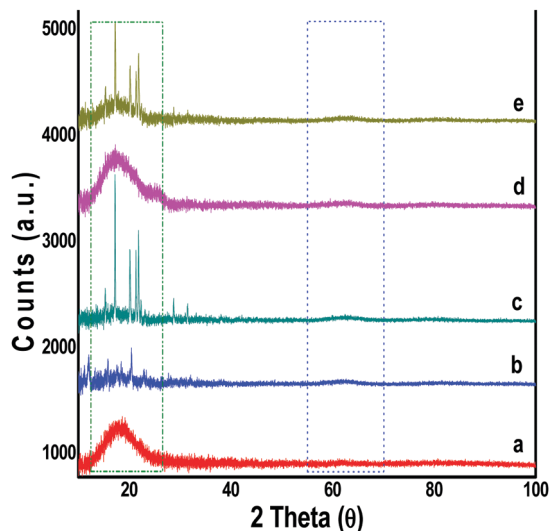
Fig. 5   XRD patterns for (a) GQDs, (b) BODIPY alone, (c) BODIPY@GQDs, (d) complex **1** alone, and (e) **1**-BODIPY@GQDs.

significant changes in the diffraction patterns with respect to the GQDs and complex **1** alone, implying only surface modification of the GQDs.

Raman spectroscopy was employed to determine the quality of the GQDs and their nanohybrids. GQDs are known to display characteristic Raman peaks termed the G-band (sp^2) tangential mode and the D-disorder band (breathing mode, sp^3). The G-band is a result of in-plane vibrations of sp^2 bonded carbon atoms, whereas the D-band is due to out-of-plane vibrations attributed to the presence of structural defects. For the GQDs alone, the characteristic G-band at 1593 cm^{-1} and D-band at 1285 cm^{-1} were observed (Fig. 6(i)).[54] As can be seen (Fig. 6(ii)), upon modification of the GQDs with the BODIPY to form BODIPY@GQDs, a large shift of the G-band to a lower frequency

(at 1495 cm^{-1}) is observed. The D-band on the other hand, was not significantly affected. The same shift applied to **1**-BODIPY@GQDs, Fig. 6(iii). Shifts in the Raman frequencies are often indicative of strong π-electron interactions in hybrid materials,[55] and increases in layer thickness hence implying formation of a new complex. Such shifts also suggest efficient charge transfer properties between the electron-donor and electron-acceptor systems.[55]

The extent of defects or quality of the graphene core can be determined by measuring the ratio of the intensities of the D and G bands (I_D/I_G). For the GQDs alone the calculated I_D/I_G was 0.16. However, upon decoration with BODIPY, D-band dominance (sp^3-type disorder) is introduced and the resultant I_D/I_G was determined to be 0.40. The I_D/I_G for **1**-BODIPY@GQDs was also 0.41. This increase in the D-band upon modification with the BODIPY confirms the increase in the structural disorder of the GQDs.[55] There is an insignificant change in the I_D/I_G ratio between BODIPY@GQDs and **1**-BODIPY@GQDs. This is because π–π interactions, unlike covalent interactions of GQDs do not result in changes in the core structure of GQDs.[26]

Photophysicochemical parameters

Fluorescence quantum yields (Φ_F) and lifetimes (τ_F). Fig. 7 shows the time-resolved florescence decay curve for **1**-BODIPY@GQDs in DMSO (as an example). Mono-exponential decay was observed in all cases. The effect of decorating the GQDs with the BODIPY dye was evaluated using the fluorescence quantum yields (Φ_F) and lifetimes (τ_F) of the GQDs (exciting where they absorb). The GQDs alone had Φ_F of 0.27 and τ_F of 3.41 ns, Table 1. Upon conjugation to complex **1**, there were slight decreases in both the Φ_F and τ_F to 0.23 and 2.84 ns for the **1**-GQDs, respectively. For the BODIPY@GQDs (when exciting where the GQDs absorbs), the Φ_F decreased to 0.02 (Table 1). It was not possible to determine the τ_F values for the GQDs and BODIPY individually in BODIPY@GQDs since the excitation laser used excited both the BODIPY and GQDs. The decrease in fluorescence quantum yields of the GQDs in the presence of complex **1** could be due to the Forster resonance energy transfer (FRET) and other processes which deactivate the excited states.[56]

When exciting where complex **1** absorbs, there is a decrease in the fluorescence quantum yields and lifetimes for **1**-BODIPY@GQDs
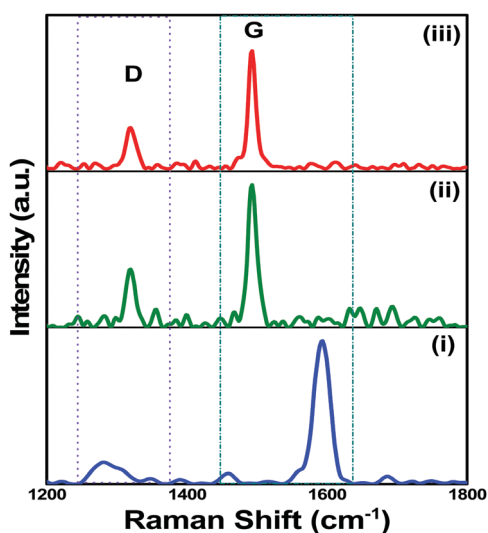

Fig. 6   Raman spectra of GQDs (i), BODIPY@GQDs (ii), and **1**-BODIPY@GQDs (iii) showing the corresponding Raman intensity changes of the GQDs upon conjugation to BODIPY and then to complex **1**.
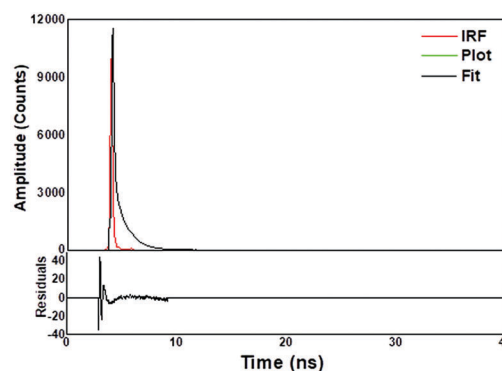

Fig. 7   Fluorescence decay curve of **1**-BODIPY@GQDs in DMSO at an excitation wavelength of 670 nm.

(at Φ_F < 0.01 and τ_F = 0.78 ns) and **1**-GQDs (at Φ_F = 0.01 and τ_F = 0.89 ns) compared to complex **1** alone (at Φ_F = 0.03 and τ_F = 1.02 ns), Table 1, due to quenching. BODIPY alone gave Φ_F = 0.85 and τ_F = 5.05 ns. The Φ_F after linking to GQDs and exciting where BODIPY absorbs for BODIPY@GQDs the Φ_F decreased to 0.60 and further to 0.55 upon conjugation to complex **1** in the **1**-BODIPY@GQDs. For the BODIPY@GQDs, FRET is expected to happen by energy transfer from the GQDs to BODIPY (not the other way around by energy considerations), hence a decrease in Φ_F (when exciting where BODIPY absorbs) cannot be attributed to FRET, but a possible heavy atom effect of sulphur in the GSH capping of the GQDs in the BODIPY@GQDs. For the **1**-BODIPY@GQDs, FRET is possible resulting in the decrease in fluorescence quantum yield when exciting where BODIPY absorbs.

Förster resonance energy transfer (FRET)

FRET involves the non-radiative transfer of energy from the donor fluorophore to an appropriate acceptor species[56] and is dependent on the spectral overlap between the donor emission and acceptor absorption. Fig. S5 (ESI†) shows the spectral overlap between the absorption spectrum of complex **1** and the emission spectra of the BODIPY and GQDs, as well the overlap of the absorption spectrum of BODIPY with the emission spectrum of GQDs. The BODIPY and BODIPY@GQDs (they both have emission spectra at the same wavelength) have a red shifted emission as compared to GQDs alone. As a result, there is stronger overlap of the BODIPY/BODIPY@GQDs emission with the absorption spectrum of **1**, compared to the GQDs. There is also overlap between the GQDs emission and BODIPY absorption. Hence FRET is expected between: (i) complex **1** (acceptor) and BODIPY (donor), (ii) complex **1** (acceptor) and GQDs (donor), and (iii) BODIPY (acceptor) and GQDs (donor).

FRET efficiency (Eff) was determined experimentally from the fluorescence quantum yields of the donor in the absence ($\Phi_{F(GQDs)}$) and presence ($\Phi_{F(GQDs)}^{Mix}$) of the acceptor using eqn (2):[31]

$$\text{Eff} = 1 - \frac{\Phi_{F(GQDs)}^{Mix}}{\Phi_{F(GQDs)}} \qquad (2)$$

For the supramolecular complexes, **1**-GQDs and **1**-BODIPY@GQDs, the Eff values obtained are 0.76 and 0.84 respectively, Table 1. It is however important to note that the obtained values are only estimates as there are a myriad of other factors that may have resulted in the decrease in the fluorescence of both the GQDs alone and BODIPY@GQDs. It is also important to note that the Eff for **1**-BODIPY@GQDs is considerably higher than that of **1**-GQDs due to the larger spectral overlap in the former seen in Fig. S5 (ESI†). The FRET efficiency in BODIPY@GQDs was determined to be 0.93. The high FRET value is due to the strong spectral overlap between the emission spectrum of GQDs and the absorption spectrum of BODIPY, Fig. S5 (ESI†), Table 1. The FRET efficiency between complex **1** and BODIPY was low at 0.69, even though the spectral overlap is the same between the complex **1** emission and the BODIPY and BODIPY@GQDs.

No significant emission peak was observed for complex **1** when it was excited at 510 nm (the wavelength used for exciting BODIPY@GQDs for FRET). There were however significant decreases in the emission intensity of BODIPY@GQDs with a small stimulated emission from complex **1** (Fig. S6, ESI†). This observation could be due to the very low fluorescence of complex **1** (Table 1).

Triplet quantum yields (Φ_T) and lifetimes (τ_T)

Triplet quantum yield (Φ_T) represents the fraction of absorbing molecules that undergo intersystem crossing to the metastable triplet excited state. The triplet state quantum yields and lifetimes for all complexes are shown in Table 1. Fig. 8 shows the triplet decay curve for complex **1** alone, **1**-GQDs, and **1**-BODIPY@GQDs in DMSO (as examples). The triplet decay curves obeyed second order kinetics, which is typical of MPcs complexes at a high concentration (1×10^{-5} M) due to the triplet–triplet recombination.[57]

From Table 1, there is a larger increase in triplet quantum yield for **1**-BODIPY@GQDs than that for **1**-GQDs. This could be as a result of the larger loading of Pcs in **1**-BODIPY@GQDs compared to **1**-GQDs. The triplet lifetimes (τ_T) of complex **1** and its nanocomposites were evaluated to determine the respective residence times of the composites in the triplet excited state. The τ_T values decreased where there was an increase in Φ_T. Intersystem crossing lifetimes τ_{ISC} (= τ_F/Φ_T) were also evaluated using the fluorescence lifetime (τ_F) and triplet quantum yields (Φ_T). The τ_{ISC} values for complex **1** and the resultant supramolecular complexes ranged from 1.00–1.59 ns. The lowest intersystem crossing lifetime was obtained for **1**-BODIPY@GQDs and may signify increased intersystem crossing to populate the triplet state in the conjugates as opposed to complex **1** alone. This subsequently translates to high triplet quantum yields observed (Table 1).

Singlet oxygen quantum yield

Singlet oxygen is formed through an energy transfer process between the excited triplet state (T_1) of MPc (^{3}MPc$\star$) and the
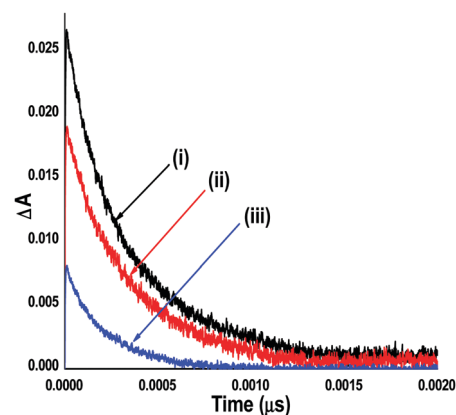

Fig. 8 Representative excited state triplet absorption decay curves of (i) complex **1** alone (ii) **1**-GQDs and (iii) **1**-BODIPY@GQDs in DMSO at an excitation wavelength of 674 nm.
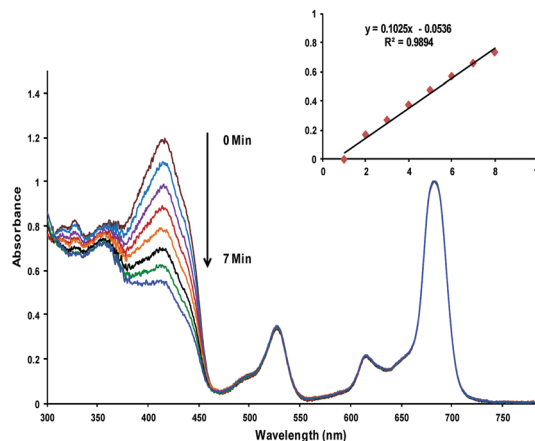
This journal is © The Royal Society of Chemistry and the Centre National de la Recherche Scientifique 2018

Fig. 9 Sample spectra showing the generation of singlet oxygen using DPBF as a single oxygen quencher for **1**-BODIPY@GQDs in DMSO.

ground state molecular oxygen ($^3O_2$). Chemical photo-degradation of the singlet oxygen quencher (DPBF) in DMSO was employed in order to determine the singlet oxygen quantum yield (Φ_Δ). Fig. 9 and Fig. S7 (ESI†) show the spectral changes observed during the photolysis of **1**-BODIPY@GQDs and BODIPY@GQDs, respectively, in DMSO, and in the presence of DPBF. The disappearance of DPBF was monitored using UV-vis spectral changes. For all the samples, the irradiation at the Q-band showed the stability of the complexes over the irradiation period.

The supramolecular complexes (**1**-GQDs and **1**-BODIPTY@GQDs) displayed an improved singlet oxygen generating ability compared to complex **1** alone, with **1**-BODIPY@GQDs having the highest Φ_Δ of 0.70. The increase in Φ_Δ corresponds to the increase in triplet state populations in going from complex **1** alone, to the supramolecular complexes **1**-GQDs and **1**-BODIPY@GQDs. There is an increase in Φ_Δ for BODIPY in the presence of the GQDs in the BODIPY@GQDs corresponding to the decrease in Φ_F. Thus, linking BODIPY to GQDs has a huge advantage as it improves their singlet oxygen generating ability.

Conclusions

In this study, the syntheses, spectral and photophysicochemical properties of BODIPY-decorated GQDs/Pcs complexes are discussed and contrasted with those of pristine GQDs/Pcs. Spectroscopic evidence shows stable supramolecular hybrids, owing to the strong π–π stacking interaction between the GQDs and the respective Pcs. The fluorescence resonance energy transfer (FRET) process of these novel conjugates was also explored in dimethyl sulfoxide. The Pc/GQD nanocomposites herein reported are characterized by a high MPcs-loading capacity and exhibited improved triplet and singlet oxygen generating ability with **1**-BODIPY@GQDs having the highest singlet oxygen value of 0.70. The obtained results are especially important as GQDs/Pcs nanocomposites such as those reported in this work, could expand and improve on areas of applications in which other carbon-based nanomaterials and their nanocomposites have achieved immense success.

Conflicts of interest

There are no conflicts to declare.

Acknowledgements

References

1 T. Nyokong and E. Antunes, in *The Handbook of Porphyrin Science*, ed. K. M. Kadish, R. M. Smith and R. Guilard, World Scientific, Singapore, 2010, vol. 7.

2 F. Steinbach and H. J. Joswig, Metal phthalocyanines used as catalysts in gas phase reactions: X. Decomposition and reduction of NO catalyzed by crystalline monomeric β-metal phthalocyanines of the first transition period, *J. Catal.*, 1978, **55**, 272–280.

3 M. Shumba, S. Centane, F. Chindeka and T. Nyokong, Nanocomposites of sulphur-nitrogen co-doped graphene oxide nanosheets and cobalt mono carboxyphenoxy phthalocyanines for facile electrocatalysis, *J. Electroanal. Chem.*, 2017, **791**, 36–48.

4 R. Zugle and T. Nyokong, Zinc(II) 2, 9, 16, 23-tetrakis [4-(*N*-methylpyridyloxy)]-phthalocyanine anchored on an electrospun polysulfone polymer fiber: Application for photosensitized conversion of methyl orange, *J. Mol. Catal. A: Chem.*, 2013, **366**, 247–253.

5 S. Harbeck, S. Göcmen, Ö. F. Emirik, Z. Z. Öztürk, V. Ahsen and A. G. Gürek, Synthesis of branched alkoxy side chains containing phthalocyanine derivates and their application in mass sensitive QCM sensors, *Sens. Actuators, B*, 2016, **233**, 55.

6 T. J. Dougherty, C. J. Gomer, B. W. Henderson, G. Jori, D. Kessel, M. Korbelik, J. Moan and Q. Peng, Photodynamic therapy, *J. Natl. Cancer Inst.*, 1998, **90**, 889–905.

7 R. Bonnett, *Chemical Aspects of Photodynamic Therapy*, Gordon and Breach, Science Publishers, Amsterdam, 2000.

8 E. Ben-Hur and I. Rosenthal, Photosensitized inactivation of Chinese hamster cells by phthalocyanines, *Photochem. Photobiol.*, 1985, **42**, 129–133.

9 B. C. Wilson and M. S. Patterson, The physics, biophysics and technology of photodynamic therapy, *Phys. Med. Biol.*, 2008, **53**, 61–109.

10 H. Jeong, M. Huh, S. J. Lee, H. Koo, I. C. Kwon, S. Y. Jeong and K. Kim, Photosensitizer-conjugated human serum albumin nanoparticles for effective photodynamic therapy, *Theranostics*, 2011, **1**, 230–239.

11 J. W. Snyder, W. R. Greco, D. A. Bellnier, L. Vaughan and B. W. Henderson, Photodynamic therapy a means to enhanced drug delivery to tumors, *Cancer Res.*, 2003, **63**, 8126–8131.

12 D. E. Dolmans, D. Fukumura and R. K. Jain, Photodynamic therapy for cancer, *Nat. Rev. Cancer*, 2003, **3**, 380–387.

13 G. Mazzone, D. A. Quartarolo and N. Russo, PDT-correlated photophysical properties of thienopyrrole BODIPY derivatives. Theoretical insights, *Dyes Pigm.*, 2016, **130**, 9–15.

14 Z. Wang, X. Hong, S. Zong, C. Tang, Y. Cui and Q. Zheng, BODIPY-doped silica nanoparticles with reduced dye leakage and enhanced singlet oxygen generation, *Sci. Rep.*, 2015, **5**, 12602–12612.

15 P. Z. Chen, H. R. Zheng, L. Y. Niu, Y. Z. Chen, L. Z. Wu, C. H. Tung. and Q. Z. Yang, A BODIPY analogue from the tautomerization of sodium 3-oxide BODIPY, *Chin. Chem. Lett.*, 2015, **26**, 631–635.

16 Y. Zhang, Y.-G. Gao, Y.-D. Shi, L.-Q. Tan, J. S. Yue and Z.-L. Lu, [12]aneN3-based BODIPY as a selective and sensitive off–on sensor for the sequential recognition of Cu2+ ions and ADP, *Chin. Chem. Lett.*, 2015, **26**, 894–898.

17 A. Kamkaew, S. H. Lim, H. B. Lee, L. V. Kiew, L. Y. Chung and K. Burgess, BODIPY dyes in photodynamic therapy, *Chem. Soc. Rev.*, 2013, **42**, 77–88.

18 S. Osati, H. Ali, E. Johan and V. Lier, Synthesis and spectral properties of phthalocyanine–BODIPY conjugates, *Tetrahedron Lett.*, 2015, **56**, 2049–2053.

19 H. Yanık, M. Göksel, S. Yeşilot and M. Durmuş, Novel phthalocyanine–BODIPY conjugates and their photophysical and photochemical properties, *Tetrahedron Lett.*, 2016, **57**, 2922–2926.

20 C. Gol, M. Malkoç, S. Yesilot and M. Durmus, Novel zinc(ɪɪ) phthalocyanine conjugates bearing different numbers of BODIPY and iodine groups as substituents on the periphery, *Dyes Pigm.*, 2014, **111**, 81–90.

21 D. Liu, F. Yang, F. Xiong and N. Gu, The smart drug delivery system and its clinical potential, *Theranostics*, 2016, **6**, 1306–1323.

22 Y. Matsumura and H. Maeda, A new concept for macromolecular therapeutics in cancer chemotherapy: mechanism of tumoritropic accumulation of proteins and the antitumor agent smancs, *Cancer Res.*, 1986, **46**, 6387–6392.

23 H. Sun, L. Wu, W. Wei and X. Qu, Recent advances in graphene quantum dots for sensing, *Mater. Today*, 2013, **11**, 433–442.

24 L. Li, G. Wu, G. Yang, J. Peng, J. Zhao and J. J. Zhu, Focusing on luminescent graphene quantum dots: current status and future perspectives, *Nanoscale*, 2013, **5**, 4015–4039.

25 Z. Fan, S. Li, F. Yuan and L. Fan, Fluorescent graphene quantum dots for biosensing and bioimaging, *RSC Adv.*, 2015, **5**, 19773–19789.

26 O. J. Achadu, I. Uddin and T. Nyokong, Interaction of graphene quantum dots grafted with polyethyleneimine and Au@Ag nanoparticles: application as fluorescence turn on nanoprobes, *J. Photochem. Photobiol., A*, 2016, **324**, 96–105.

27 D. Qu, M. Zheng, P. Du, Y. Zhou, L. Zhang, D. Li, H. Tan, Z. Zhao, Z. Xied and Z. Sun, Highly luminescent S, N co-doped graphene quantum dots with broad visible absorption bands for visible light photocatalysts, *Nanoscale*, 2013, **5**, 12272–12277.

28 J. Dong, K. Wang, L. Sun, B. Sun, M. Yang, H. Chena, Y. Wang, J. Sun and L. Dong, Application of graphene quantum dots for simultaneous fluorescence imaging and tumor-targeted drug delivery, *Sens. Actuators, B*, 2018, **256**, 616–623.

29 H. W. Yang, C. Y. Huang, C. W. Lin, H. L. Liu, C. W. Huang, S. S. Liao, P. Y. Chen, Y. J. Lu, K. C. Wei and C. C. Ma, Gadolinium-functionalized nanographene oxide as a nanocarrier for combined drug and microRNA delivery and magnetic resonance imaging, *Biomaterials*, 2014, **35**, 6534–6542.

30 J. Ge, M. Lan, B. Zhou, W. Liu, L. Guo, H. Wang, Q. Jia, G. Niu., X. Huang, H. Zhou, X. Meng, P. Wang, C.-S. Lee, W. Zhang and X. Han, A graphene quantum dot photodynamic therapy agent with high singlet oxygen generation, *Nat. Commun.*, 2014, **5**, 4596–4603.

31 O. J. Achadu and T. Nyokong, Graphene quantum dots coordinated to mercaptopyridine-substituted phthalocyanines: Characterization and application as fluorescence "turn ON" nanoprobes, *Spectrochim. Acta, Part A*, 2017, **174**, 339–347.

32 N. Nwahara, J. Britton and T. Nyokong, Improving singlet oxygen generating abilities of phthalocyanines: aluminium tetrasulfonated phthalocyanine in the presence of graphene quantum dots and folic acid, *J. Coord. Chem.*, 2017, **70**, 1601–1616.

33 D. Dei, G. Chiti, M. P. De Filippis, L. Fantettia, F. Giuliani, F. Giuntini, M. Soncin, G. Jori and G. Roncucci, Phthalocyanines as photodynamic agents for the inactivation of microbial pathogens, *J. Porphyrins phthalocyanines*, 2006, **10**, 147–159.

34 A. Fashina, E. Antunes and T. Nyokong, Characterization and photophysical behavior of phthalocyanines when grafted onto silica nanoparticles, *Polyhedron*, 2013, **53**, 278–285.

35 S. Banfi, G. Nasini, S. Zaza and E. Caruso, Synthesis and photo-physical properties of a series of BODIPY dyes, *Tetrahedron*, 2013, **69**, 4845–4856.

36 S. Fery-Forgues and D. Lavabre, Are Fluorescence Quantum Yields So Tricky to Measure? A Demonstration Using Familiar Stationery, *J. Chem. Educ.*, 1999, **76**, 1260–1264.

37 A. Ogunsipe, J. Chen and T. Nyokong, Photophysical and photochemical studies of zinc(ɪɪ) phthalocyanine derivatives—effects of substituents and solvents, *New J. Chem.*, 2004, **28**, 822–827.

38 A. M. Brouwer, Standards for photoluminescence quantum yield measurements in solution (IUPAC Technical Report), *Pure Appl. Chem.*, 2011, **83**, 2213–2228.

39 H. Lu., J. Mack, Y. Yang and Z. Shen, Structural modification strategies for the rational design of red/NIR region BODIPYs, *Chem. Soc. Rev.*, 2014, **43**, 4778–4823.

40 T. H. Tran-Thi, C. Desforge and C. Thiec, Singlet-singlet and triplet-triplet intramolecular transferprocesses in a covalently linked porphyrin-phthalocyanine heterodimer, *J. Phys. Chem.*, 1989, **93**, 1226–1233.

41 M. Morisue, S. Ueda, M. Kurasawa, M. Naito and Y. Kuroda, Highly fluorescent slipped-cofacial phthalocyanine dimer as

a shallow inclusion complex with α-cyclodextrin, *J. Phys. Chem. A*, 2012, **116**, 5139–5144.

42 Z. Zhu, J. Qian, X. Zhao, W. Qin, R. Hu, H. Zhang, D. Li, Z. Xu, Z. B. Tang and S. He, Stable and Size-Tunable Aggregation-Induced Emission Nanoparticles Encapsulated with Nanographene Oxide and Applications in Three-Photon Fluorescence Bioimaging, *ACS Nano*, 2016, **10**, 588–597.

43 X. Hong, Z. Wang, J. Yang, Q. Zheng, S. Zong, Y. Sheng, D. Zhu, C. Tang and Y. Cui, Silylated BODIPY dyes and their use in dye-encapsulated silica nanoparticles with switchable emitting wavelengths for cellular imaging, *Analyst*, 2012, **137**, 4140–4149.

44 X. Wu, F. Tian, W. Wang, J. Chen, M. Wu and J. X. Zhao, Fabrication of highly fluorescent graphene quantum dots using ʟ-glutamic acid for *in vitro/in vivo* imaging and sensing, *J. Mater. Chem. C*, 2013, **31**, 4676–4684.

45 L. K. Limbach, Y. Li, R. N. Grass, T. J. Brunner, M. A. Hintermann, M. Muller, D. Gunther and W. J. Stark, Oxide nanoparticle uptake in human lung fibroblasts: effects of particle size, agglomeration, and diffusion at low concentrations, *Environ. Sci. Technol.*, 2005, **39**, 9370–9376.

46 S. Zhu, J. Shao, Y. Song, X. Zhao, J. Du, L. Wang, H. Wang, K. Zhang, J. Zhang and B. Yang, Investigating the surface state of graphene quantum dots, *Nanoscale*, 2015, **7**, 7927–7933.

47 L. Li, J. F. Zhao, N. Won, H. Jin, S. Kim and J. Y. Chen, Quantum dot-aluminum phthalocyanine conjugates perform photodynamic reactions to kill cancer cells *via* fluorescence resonance energy transfer, *Nanoscale Res. Lett.*, 2012, **7**, 386–393.

48 L. Li, G. Wu, G. Yang, J. Peng, J. Zhao and J. J. Zhu, Focusing on luminescent graphene quantum dots: current status and future perspectives, *Nanoscale*, 2013, **5**, 4015–4039.

49 B. D. Shinde and V. K. Pillai, Electrochemical Preparation of Luminescent Graphene Quantum Dots from Multiwalled Carbon Nanotubes, *Chem. – Eur. J.*, 2012, **18**, 12522–12528.

50 S. Wang, R. Tan, Y. Li, Q. Li and S. Xiao, Solid state emission and mechanochromic luminescence of boron 2-(2′-pyridyl)-imidazole complexes, *Dyes Pigm.*, 2016, **132**, 342–346.

51 J. C. Yu, W. Ho, J. Yu, S. K. Hark and K. Iu, Effects of Trifluoroacetic Acid Modification on the Surface Micro-structures and Photocatalytic Activity of Mesoporous TiO$_2$ Thin Films, *Langmuir*, 2003, **19**, 3889–3896.

52 Z. L. Yang, H. Z. Chen, L. Cao, H. Y. Li and M. Wang, Synthesis and photoconductivity study of carbon nanotube bonded by tetrasubstituted amino manganese phthalo-cyanine, *Mater. Sci. Eng., B*, 2004, **106**, 73–78.

53 R. Prabakaran, R. Kesavamoorthy, G. L. N. Reddy and F. P. Xavier, Structural investigation of copper phthalocya-nine thin films using X-ray diffraction, raman scattering and optical absorption measurements, *Phys. Status Solidi*, 2002, **229**, 1175–1186.

54 A. C. Ferrari and J. Robertson, Resonant Raman Spectro-scopy of disordered, amorphous, and diamondlike carbon, *Phys. Rev. B: Condens. Matter Mater. Phys.*, 2001, **61**, 1–13.

55 Z. Li, C. He, Z. Wang, Y. Gao, Y. Dong, C. Zhao, Z. Chen, Y. Wu and W. Song, An Ethylenediamine-Modified Graphene Oxide Covalently Functionalized with Tetracarboxylic Zn(ɪɪ) Phthalocyanine Hybrid for Enhanced Nonlinear Optical Properties, *Photochem. Photobiol. Sci.*, 2016, **15**, 910–919.

56 C. Berney and G. Danuser, FRET or No FRET: a quantitative comparison, *Biophys. J.*, 2003, **84**, 3992–4010.

57 M. G. Debacker, O. Deleplanque, V. B. Vlierberge and F. X. Sauvage, A Laser Photolysis Study of Triplet Lifetimes and of Triplet–Triplet Annihilation Reactions of Phthalo-cyanins in DMSO Solutions, *Laser Chem.*, 1988, **8**, 1–11.